Available online at www.sciencedirect.com
SCIENCE DIRECT®
Journal of Catalysis 227 (2004) 68–76
JOURNAL OF CATALYSIS
www.elsevier.com/locate/jcat

Simultaneous determination of the pore-length distribution and pore connectivity for porous catalyst supports using integrated nitrogen sorption and mercury porosimetry

Sean P. Rigby [a,*], Matthew J. Watt-Smith [a], Robin S. Fletcher [b]

[a] *Department of Chemical Engineering, University of Bath, Claverton Down, Bath, BA2 7AY, UK*
[b] *Johnson Matthey Catalysts, PO Box 1, Belasis Avenue, Billingham, Cleveland, TS23 1LB, UK*

Received 13 February 2004; revised 8 June 2004; accepted 30 June 2004

Available online 23 July 2004

Abstract

Well-known and standard techniques exist for the determination, from gas sorption data, of key characteristic parameters of porous heterogeneous catalysts, such as the specific surface area (BET), pore-diameter distribution (BJH), and pore connectivity (percolation analysis). However, at present, there are no methods to determine the pore-*length* distribution. Many previous mathematical modelling studies have shown that the nature of the relationship that exists between pore diameter and pore length heavily influences the rate of mass transport processes in porous solids, such as heterogeneous catalysts. Hence, a major obstacle to the proper implementation of pore-network models to study coupled diffusion and reaction processes in catalysts is the lack of a method for determining the pore-length distribution. This paper presents a new analytical method to determine the pore-length distribution from the results of novel experiments using the recently introduced integrated nitrogen sorption and mercury porosimetry technique. The analysis also, simultaneously, delivers improved estimates of pore connectivity and lattice size.

Keywords: Pore-length distribution; Catalyst support; Nanostructure; Gas sorption; Mercury porosimetry; Percolation theory; Pore connectivity

1. Introduction

Mesoporous solids with complex internal void space geometries are frequently used in industry as supports for heterogeneous catalysts and as absorbents. Such solids include materials such as sol–gel silica spheres, and alumina tablets or extrudates. The performance of these materials, in the duties in which they are employed, often depends upon the rate of transport processes within their internal void space. Therefore, in order to design a particular industrial process, it is necessary to be able to predict the rate of mass transport in complex porous solids. Hence, it is necessary to characterise the void space of the porous solids to a sufficient degree to be able to construct a fully predictive structural model. A potential example of such a model pore structure is the random pore-bond network. This type of model consists of a lattice where (typically) cylindrical or slit-shaped pore elements lie along some, or all, of the lattice bonds, which meet at the lattice nodes. The key characteristic parameters of pore-bond networks are the surface area, porosity, pore-size distribution (the probability density function of pore diameter weighted by volume), pore connectivity, overall lattice size, and *also* the pore-length distribution. In this context, pore connectivity is defined as the overall average number of pores that meet at a typical pore junction. Well-established methods exist for the determination of the specific surface area or pore-diameter distribution of a porous solid from a nitrogen adsorption isotherm, using either thermodynamic [1–3] or statistical mechanical [4] methods. Several sets of workers [5–8] have also presented methods to determine the pore connectivity

* Corresponding author.
E-mail address: s.p.rigby@bath.ac.uk (S.P. Rigby).

0021-9517/$ – see front matter
doi:10.1016/j.jcat.2004.06.025

and lattice size from either nitrogen sorption or mercury porosimetry alone. The above characteristic parameters are often used for correlating various aspects of catalyst performance with structural properties. However, there are no general methods for determining the pore-*length* distribution for a random pore-bond network model using nitrogen sorption and/or mercury porosimetry. This lack of a suitable technique prevents the proper implementation of pore-bond network models to successfully predict transport phenomena, or coupled diffusion and reaction, in porous media. It is the purpose of this paper to present such a method. It is also anticipated that the pore-length distributions obtained using the method described below may be useful in understanding the relative performance of different catalysts, and, in particular, their resistance to coking and pellet strength.

Recent work [9,10] demonstrates that pore-bond networks are accurate representations of the structure of the void space of porous media. Light-scattering studies [9,10] have been made of the adsorption and desorption of hexane in porous Vycor glass. Since the pores in empty Vycor are very small (~ 5 nm), the material appears homogeneous on length scales comparable with the wavelength of light, and thus scatters light very weakly. On filling the void space with hexane during adsorption, the measured transmission of light was roughly independent of the pressure. When the pores are completely saturated with fluid, there is virtually no mismatch in the index of refraction, and the scattering is reduced even further. However, during desorption, the transmission exhibited a very sharp and narrow dip due to the strong scattering of light occurring at hexane pressures corresponding to the steep step decline in the desorption isotherm. During desorption, as the Vycor drains, only some pores are emptied at first. At this stage, all of the surrounding pores are still filled with fluid and are thus index-matched to the glass, and hence they do not contribute to the scattering. There is thus a large scattering contrast between the regions of empty pores and the remaining Vycor, where the pores are still full. The difference in the degree of scattering, between adsorption and desorption, was attributed to the development of large-scale inhomogeneities in the spatial distribution of empty pores which were comparable in size with the wavelength of light, and, thus, could cause an increase in scattering. These correlations were found to have a fractal dimension of 2.6, which is very near the value of 2.5 predicted for an invasion percolation process (such as gas desorption) in a 3D pore-bond network. This work demonstrates that 3D random pore-bond networks can provide a realistic description of the pore structure of some porous media.

Random pore-bond networks have been used to study pressure swing adsorption [11], and coupled diffusion and reaction processes within porous heterogeneous catalyst pellets [12–14]. This work has been extended to include the effects (on transport and reaction) of solid deposition from processes such as coking [15], and the presence of condensable vapours [16]. The use of pore-bond network models allows the testing of the influence of various aspects of the pore structure of the catalyst support, such as pore connectivity, on the performance of a particular catalyst system. This modelling work can then be used to propose the most appropriate pore structure for a given catalyst, and design the reactor for a particular catalytic process. However, mathematical modelling, using pore-bond networks, of gas-solid reactions within porous media that produce solid products has shown that the pore-length distribution strongly influences the model predictions [17]. Simulations of the intrusion and retraction of nonwetting fluids, such as mercury, in pore-bond networks have also shown that the relationship between pore diameter and pore length has a significant effect on the process [18]. There is thus a need to be able to measure all of the appropriate characteristic parameters of the pore network of real materials, including the pore-length distribution.

The particular analysis method, to determine pore connectivity and lattice size from nitrogen sorption data, originally developed by Seaton and co-workers [8,19,20] has subsequently been extended to account for the spatial distribution of pore connectivity [21], for use with macroporous samples [22], and to substitute mercury intrusion for nitrogen desorption data [23]. This analysis method implicitly uses both the “pore-blocking” theory of nitrogen sorption hysteresis [24] and percolation theory [25]. The essence of the pore-blocking theory is that, during desorption, nitrogen can only vaporise from a given pore if there is a continuous path of vapour-filled pores that leads all of the way from the pore in question to the surface of the sample. The formation of this path, which corresponds to the “knee” in the desorption isotherm, is described by percolation theory. The validity of the pore-blocking theory for the desorption of nitrogen from mesoporous solids has been demonstrated using the integrated nitrogen sorption and mercury porosimetry method [26]. In this technique [27], nitrogen sorption isotherms are obtained both before and after a mercury porosimetry experiment on the same sample by freezing in place the mercury that becomes entrapped during porosimetry. In the work to be presented here, the results of experiments, using the recently introduced [27] integrated nitrogen sorption and mercury porosimetry technique, have been analysed using a novel theoretical approach, partly based on the original method developed by Seaton [8], that is suitable for application to the particular dataset emerging from an integrated experiment. The much larger amount of information about a porous solid that it is possible to derive from integrated nitrogen sorption and mercury porosimetry experiments, when compared to either technique used alone, allows the new analysis method presented here to simultaneously determine the pore-length distribution, lattice size, and pore connectivity for a random pore-bond network model of the sample.

2. Theory

2.1. Suitability of a sample for application of the theory

In the new theory presented here it is assumed that if mercury becomes entrapped within a particular pore in the network following porosimetry, then that pore is completely filled with mercury. It is also assumed that if mercury retracts from a given pore, then it completely empties that pore. This type of mechanism of mercury extrusion is known as "piston-type retraction," and is commonly assumed in simulations of mercury porosimetry in random pore-bond network models [28,29]. This is because mercury porosimetry experiments on glass micromodels consisting of pore-bond networks etched in glass show the piston-type intrusion and retraction behaviour [30]. However, porosimetry experiments on glass micromodels consisting of different networks of relatively wide pore bodies connected by narrow pore necks have shown that entrapped mercury may only partially fill a pore body within which it becomes entrapped [30]. Therefore, instead of mercury entrapment leading to the complete loss of a relatively large pore, it is, instead, "converted" into a smaller pore. It is, therefore, necessary to distinguish which of these two scenarios is occurring in order to decide whether the new analysis given below is applicable to a given sample. The suitability of the new approach can be determined by comparing the BJH [2] pore-diameter distributions obtained from nitrogen adsorption before and after mercury porosimetry. If larger pore bodies are only becoming partially filled with entrapped mercury during porosimetry, then the volume of larger pores in the BJH [2] pore-diameter distribution will decrease, while the volume of smaller pores will appear to increase. This is accompanied by an overall loss in total pore volume. The type of shift in the BJH [2] pore-diameter distribution following porosimetry, where partial entrapment is occurring, is illustrated in Fig. 1. The cumulative pore-diameter distribution obtained after porosimetry shown in Fig. 1 has been renormalised such that the ultimate volume is the same as that before porosimetry. This way of presenting the data makes the loss of larger pores more apparent. In contrast, if piston-type retraction of mercury is occurring, and the larger pores that entrap mercury are completely filled with metal, then, in the pore-diameter distribution, only the volumes of pores that entrap mercury will decrease. The incremental volumes of no pores of any diameter will appear to increase. If only the largest pores in the network entrap mercury, then the volume of these pores will decrease while the rest of the pore-diameter distribution remains unaltered. This scenario is illustrated in Fig. 2. Again, the cumulative pore-diameter distribution obtained after porosimetry shown in Fig. 2 has been renormalised such that the ultimate volume is the same as that before porosimetry to make the loss of only the larger pores more apparent. In order for the analysis described below to be appropriate the mercury must retract by a piston-type mechanism, as in the second scenario described above.

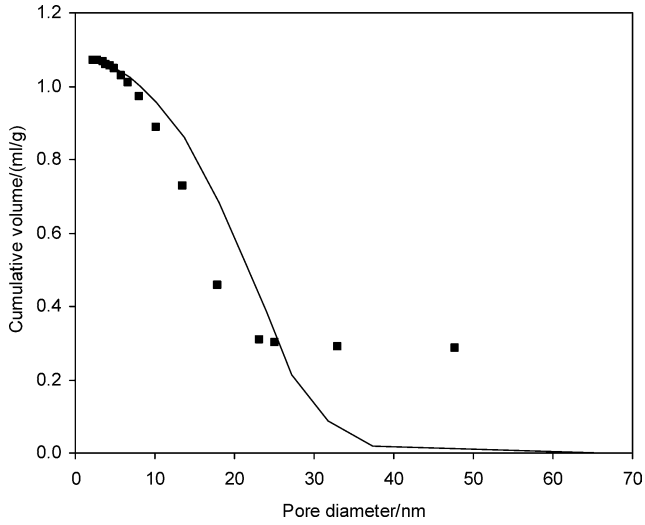

Fig. 1. Cumulative pore-diameter distributions, derived using the BJH algorithm, from the nitrogen adsorption isotherms obtained before (solid line) and after (■) mercury porosimetry for a sample of sol–gel silica spheres from batch P4.

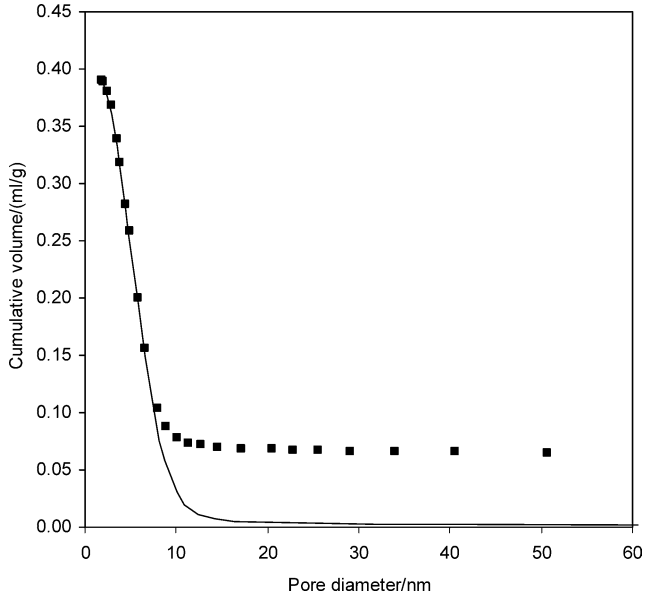

Fig. 2. Cumulative pore-diameter distributions, derived using the BJH algorithm, from the nitrogen adsorption isotherms obtained before (solid line) and after (■) mercury porosimetry for a sample of sol–gel silica spheres from batch Q2.

The new analysis method described below also assumes that the number of nodes (vertices) in the network remains the same before and after porosimetry. This means that the network does not become separated into two disjoint sub-networks by a complete barrier of entrapped mercury. In addition, it is also assumed that two, or more, empty pores joining at a particular common node retain direct communication between themselves via that node, and the entrapped mercury within other adjacent, but still filled, pores does not lead to a constriction causing additional pore-blocking effects. This assumption is reasonable since it is what is com-

monly observed in porosimetry experiments on micromodels consisting of pore-bond networks etched in glass [30]. Wardlaw and McKellar [30] have shown that generally, when two, or more, empty, adjacent pore bonds join at a specific node, they maintain direct communication via that node even when other pore bonds attached to the same node are still filled with entrapped mercury.

2.2. Percolation analysis

As noted above, the new analysis presented here is a substantial modification of the original percolation method developed by Seaton [8]. This section describes in detail the novel aspects of the new analysis method. For more information on the more basic percolation analysis the reader is referred the original reference [8].

As in the original percolation method [8,22] the analysis presented here is carried out in terms of percolation variables, the values of which are calculated from pore-diameter distributions (obtained from nitrogen adsorption isotherms), and the adsorption and desorption isotherms themselves. The bond occupation probability at a particular pressure is given by

$$X = \frac{\text{The number of pores below their condensation pressure}}{\text{The total number of pores in the network}}. \tag{1}$$

X represents the number fraction of pores that would have emptied in a perfectly connected network. Assuming cylindrical pores, the pore-number distribution as a function of pore-diameter is calculated from the conventional BJH [2] pore-diameter distribution obtained from the nitrogen adsorption isotherm. The number, n_i, of pores of diameter d_i is given by

$$n_i = \frac{V_i}{(\pi/4)d_i^2 l_i}, \tag{2}$$

where V_i is the total volume of pores with diameter d_i, and l_i is the average pore-length for pores of diameter d_i.

The set of X values (one for each data point on the desorption, isotherm) is then given by

$$X_i = \frac{\sum_{j=1}^{i} n_j}{T} = \frac{\sum_{j=1}^{i} n_j}{\sum_{j=1}^{N} n_j}, \tag{3}$$

where T is the total number of pores in the network, and N is the number of pore-size intervals. In the original percolation analysis method of Seaton and co-workers [8] it was assumed that the average pore length l_i is the same in each pore-size interval. Hence, since n_i occurs in both the numerator and the denominator of Eq. (3), then there was previously no need to actually assign a value to l_i. However, in the new analysis method presented here, it is assumed that the average pore length, l_i, of pores of diameter, d_i, is a function of the pore diameter, such that the distribution of average pore length for each pore diameter follows a power law,

$$l_i = k \cdot d_i^{\alpha}, \tag{4}$$

where k and α are constants that characterise the shape of the particular distribution of average pore length with pore diameter for the material under study. In the new analysis only the constant k cancels from both the denominator and numerator in Eq. (3).

The accessibility, X^{A}, is the number fraction of pores that are both below their condensation pressure and have access to the surface, either directly or via a network of vapour-filled pores

$$X^{\mathrm{A}} = \frac{\text{The number of pores from which nitrogen has vapourised}}{\text{The total number of pores in the network}}. \tag{5}$$

Hence, in other words, X^{A} is the fraction of pores from which desorption has actually occurred. The experimental values of X^{A} (as a function of pressure, or, equivalently, X) are calculated from the deviation between the adsorption and desorption isotherms according to the method described previously by Seaton [8]. As is completely reasonable for a random pore-bond network, the original method [8] for the calculation of X^{A} assumes that the respective pore-size distributions for both the set of pores from which nitrogen has actually vapourised and the set of pores that are below their condensation pressure but from which nitrogen has not yet desorbed are the same. The same assumption will be made here. However, a method for correcting the original percolation analysis [8], using magnetic resonance images, for materials where this assumption does not hold has been given in previous work [31]. The experimentally derived pairs of values of X and X^{A} are then fitted to a universal scaling relation

$$L^{\beta/\nu} Z X^{\mathrm{A}} = G\big\lfloor (ZX - 3/2) L^{1/\nu} \big\rfloor, \tag{6}$$

where β and ν are critical exponents which take values of 0.41 and 0.88, respectively. The generalised scaling relation G was constructed using the simulation data of Kirkpatrick [32]. This relationship makes use of the universal relationship between Z and the value of X at the percolation threshold, X_c:

$$Z X_c = 1.5. \tag{7}$$

The fitted values of Z and L are the estimates of the connectivity and lattice size of the sample.

In the new method presented here, the above percolation analysis is performed on the nitrogen sorption data obtained both before and after mercury porosimetry in an integrated experiment. During mercury extrusion from most samples some mercury becomes permanently entrapped within the void space. Thus, mercury entrapment leads to the blocking of some of the pores in the network. The presence of mercury in certain pore bonds then completely prevents access of nitrogen to those particular bonds in the subsequent

sorption experiment. Hence, following porosimetry, the entrapped mercury leads to a decrease in the number of accessible pores, and, hence, also a decrease in the connectivity of the network. The lattice size will remain constant provided insufficient mercury has become entrapped to disconnect the pore network into two completely separate parts. For large lattices, as long as the number fraction of pores occupied by entrapped mercury is below the percolation threshold, the lattice is certain to remain fully connected.

Besides being given by the denominator in Eq. (3), the total number of pore bonds in the network, T, is also given by

$$T = Z \times (\text{the total number of nodes in the network})/2. \quad (8)$$

The factor 2 in Eq. (8) originates from the fact that each pore connects two nodes. Since the number of nodes in the network (and thus the overall lattice size, L) does not change following mercury porosimetry, the ratio of the total numbers of open pores before and after porosimetry is given by

$$\frac{T_A}{T_B} = \frac{\sum_{j=1}^{N} \frac{V_{A,j}}{d_j^{(2+\alpha)}}}{\sum_{j=1}^{N} \frac{V_{B,j}}{d_j^{(2+\alpha)}}} = \frac{Z_A}{Z_B}, \quad (9)$$

where the subscripts B and A, refer to quantities obtained before and after porosimetry, respectively. The summations in the numerator and denominator in Eq. (9) are carried out over identical sets of pore-size intervals. The requirement for a constant lattice size before and after porosimetry (i.e., $L_A = L_B$), and the condition given by Eq. (9) represent additional constraints on the particular values of Z and L that are obtained from the percolation analysis of the nitrogen sorption data from both before and after porosimetry. These extra constraints ensure that the model parameters obtained before and after porosimetry are internally consistent within the theory. In addition, the above two extra conditions, which preserve the internal consistency of the percolation theory when applied to integrated nitrogen sorption and mercury porosimetry experiments, constrain the model further such that the additional adjustable parameter α, introduced in the new analysis, may also be determined. Hence, the new analysis allows the determination of the parameter α, and thus the pore-length distribution. The connectivity obtained using the universal scaling relation Eq. (6) is the mean value averaged over all of the *accessible* nodes in the network. The derivation of Eq. (9) from Eq. (8) assumes that the number of open nodes remains constant following porosimetry. Hence, if the connectivity obtained using Eq. (6) is used in Eq. (9), then the condition,

$$\left[1 - \left(\frac{T_A}{T_B}\right)\right]^{Z_B} \cdot (L-3)^3 < 1, \quad (10)$$

should also be, at least, approximately satisfied. The factor $(L-3)^3$ arises in Eq. (10), rather than $(L+1)^3$, because the nodes close to the outer boundary of the lattice remain permanently accessible. If significant numbers of nodes become completely disconnected from the network, as would arise with relatively high levels of mercury entrapment, an alternative to Eq. (6) must be used to determine the connectivity appropriate for use in Eq. (9).

In order to calculate k, in addition to α, it is assumed that the pore-bond network has a random, rather than regular, pattern similar to the model described by Mann et al. [18]. The introduction of variable pore lengths while maintaining topological integrity for an interconnected set of pores is achieved by a simple modification of the regular network. Each node in the network is assumed to be surrounded by a cube of side-length the same as the spacing in a regular network occupying the same overall volume. In a regular network each node would be located at the centre of its surrounding cube. In the random pattern network each node is assumed to be randomly located somewhere within its surrounding cube. The random positioning of the nodes means that the direct path between one side of a network and the other is no longer a straight line following the axis of the pore bonds, as it would be in a regular pore network. The pathway is more tortuous, in that it is of an additional length compared to a regular network. Monte Carlo simulations of pore positions in a 3D random pattern pore-bond network suggest that this tortuosity τ has a value of 1.1676 ± 0.0002. The overall, characteristic linear dimension of the lattice, D (e.g., the side-length of a cubic, solely mesoporous pellet), is thus given by

$$D = \frac{L \cdot \bar{l}}{\tau}, \quad (11)$$

where

$$\bar{l} = \frac{\sum_{i=1}^{N} l_i \cdot n_{B,i}}{T_B} = \frac{k \sum_{i=1}^{N} V_{B,i} \cdot d_i^{-2}}{\sum_{i=1}^{N} \frac{V_{B,i}}{d_i^{(2+\alpha)}}}, \quad (12)$$

and is the average pore-length weighted by number of pores. Hence the parameter k of the pore-length distribution is given by

$$k = \frac{\frac{D\tau}{L} \sum_{i=1}^{N} \frac{V_{B,i}}{d_i^{(2+\alpha)}}}{\sum_{i=1}^{N} V_{B,i} \cdot d_i^{-2}}. \quad (13)$$

3. Experimental

Samples for the experiments each consisted of a small number of sol–gel silica catalyst support pellets taken from two different batches denoted Q2 and W1. Nitrogen sorption experiments were carried out at 77 K using a Micromeritics ASAP 2400 apparatus. The sample tube and its contents were loaded into the degassing port of the apparatus and initially degassed at room temperature until a vacuum of 0.27 Pa was recorded. A heating mantle was then applied to the sample tube and the contents were heated, under vacuum, to a temperature of 623 K. The sample was then left under

vacuum for 14 h at a pressure of 0.27 Pa. The purpose of the thermal pretreatment for each particular sample was to drive off any physisorbed water on the sample but to leave the morphology of the sample itself unchanged. A range of different thermal pretreatment procedures was considered in order to determine whether the experimental results were sensitive to the temperature or time period used. This was found not to be the case. For all samples, at this point the heating mantle was removed and the sample allowed to cool down to room temperature. The sample tube and its contents were then reweighed to obtain the dry weight of the sample before being transferred to the analysis port for the automated analysis procedure. The sample was then immersed in liquid nitrogen at 77 K before the sorption measurements were taken. The adsorption isotherms obtained were analysed using the BJH [2] method to obtain the pore-diameter distributions. The film thickness for multilayer adsorption was taken into account using the well-known Harkins and Jura equation [24]. In the Kelvin equation [24] the adsorbate property factor was taken as 9.53×10^{-10} m and it was assumed that the fraction of pores open at both ends was 0.0. It was, therefore, assumed that capillary condensation commenced at the closed end of a pore to form a hemispherical meniscus.

Following the first nitrogen sorption experiment, the sample was allowed to reach room temperature (298.9 K) and then transferred to the mercury porosimeter still under nitrogen. Mercury porosimetry experiments were performed using a Micromeritics Autopore IV 9420. The sample was first evacuated to a pressure of 6.7 Pa in order to remove physisorbed gases from the interior of the sample. The standard equilibration time used in the experiments was 15 s. When the raw data were analysed according to the Washburn equation the value taken for the surface tension of mercury was 0.485 N m^{-1}. The corresponding values for the advancing and receding contact angles were both taken as 140°. Since it is difficult to thoroughly clean entrapped mercury from a given sample after an experiment for reuse in a further mercury porosimetry experiment, each particular set of experiments was, instead, repeated on several samples from the same batch. Following mercury porosimetry the sample was transferred back to the nitrogen sorption apparatus. The sample was then cooled to 77 K to freeze the mercury in place. Following the cooling of the sample, it was evacuated to vacuum and the next nitrogen sorption experiment commenced.

4. Results and discussion

Integrated nitrogen sorption and mercury porosimetry experiments were performed on two samples taken from batches Q2 and W1. The nitrogen sorption isotherms obtained before and after porosimetry for batches Q2 and W1 are shown in Figs. 3 and 4, respectively. The mercury porosimetry data are shown in Fig. 5. The small initial rise in the intrusion curves, at pore diameters of ∼ 100 μm, is

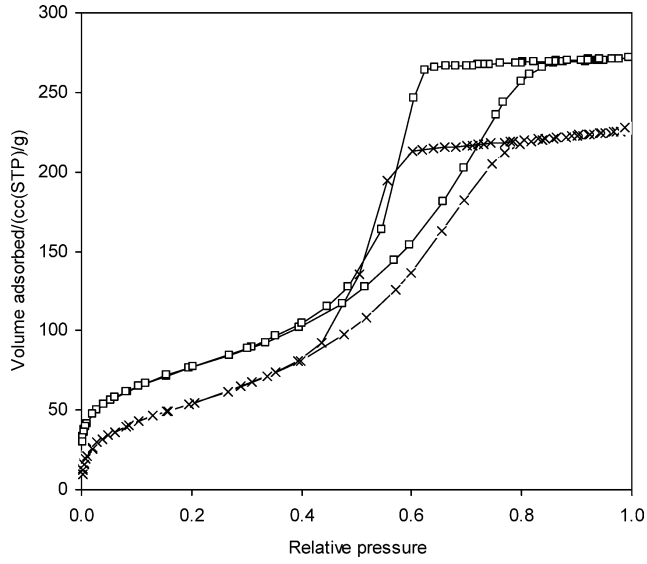

Fig. 3. Nitrogen sorption isotherms obtained before (□) and after (×) mercury porosimetry for a sample of sol–gel silica spheres from batch Q2.

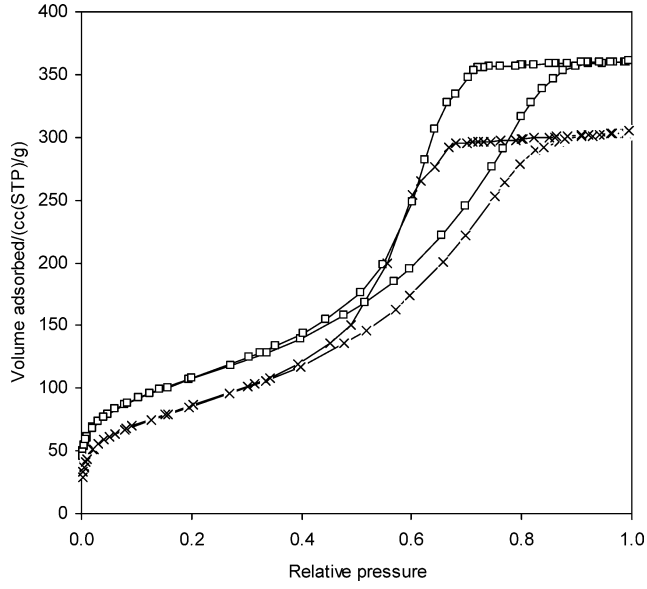

Fig. 4. Nitrogen sorption isotherms obtained before (□) and after (×) mercury porosimetry for a sample of sol–gel silica spheres from batch W1.

probably due to interparticle intrusion within the gaps between pellets. It can be seen that the entrapment of mercury, observed in Fig. 5, leads to a loss of accessible pore volume in the sorption isotherms. *t*-Plot analyses of the adsorption isotherms confirm that, in each case, the contraction of the mercury during cooling to 77 K does not lead to the creation of microporous cracks into which nitrogen can fit. Superimposed pore-diameter distributions derived, using the BJH [2] algorithm, from the adsorption isotherms obtained before and after porosimetry are shown in Figs. 2 and 6 for batches Q2 and W1, respectively. In each case, the ultimate volume of the cumulative diameter distribution obtained after porosimetry has been adjusted to be the same as that

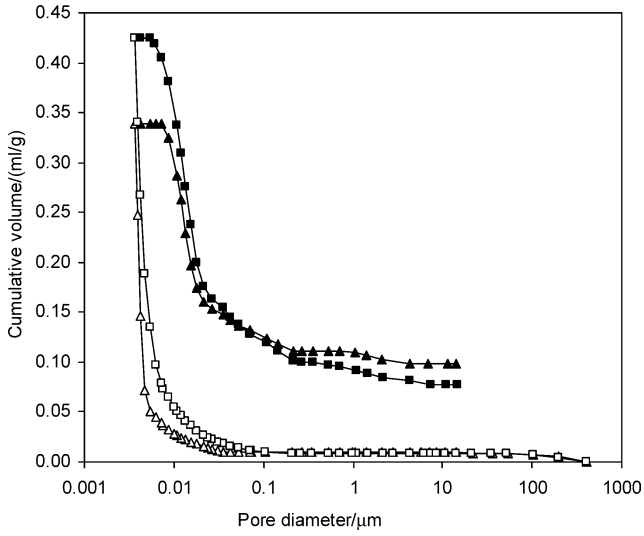

Fig. 5. Mercury intrusion (open symbols) and extrusion (solid symbols) curves for samples from batch Q2 (▲) and W1 (■).

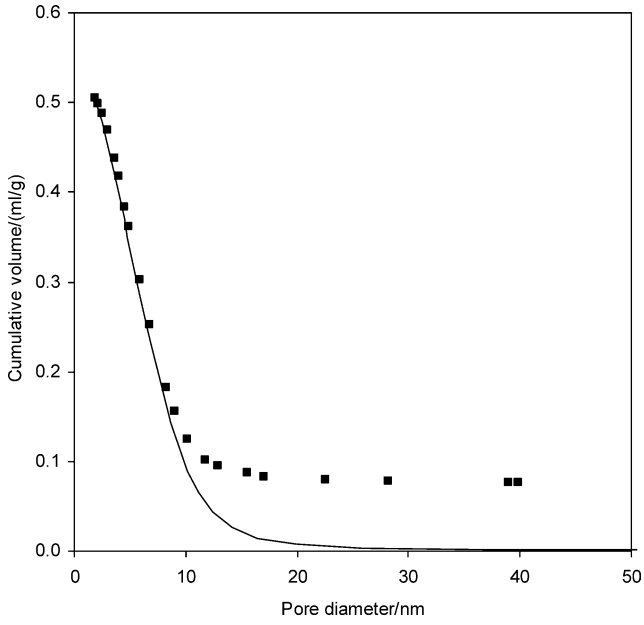

Fig. 6. Cumulative pore-diameter distributions, derived using the BJH algorithm, from the nitrogen adsorption isotherms obtained before (solid line) and after (■) mercury porosimetry for a sample of sol–gel silica spheres from batch W1.

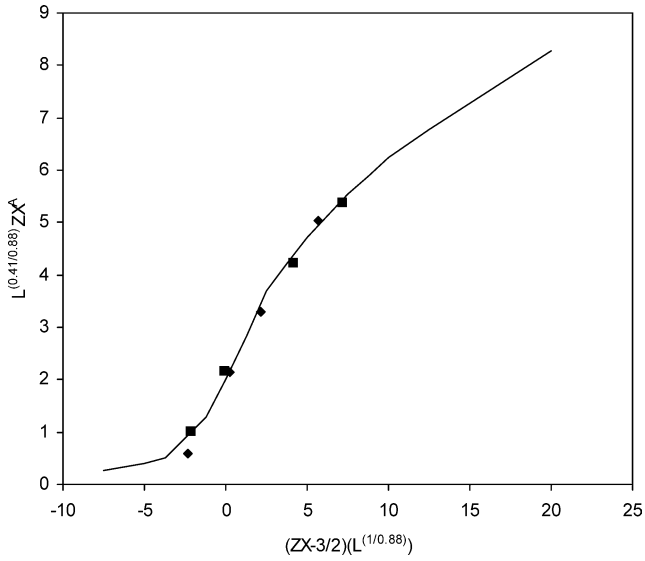

Fig. 7. Fits to the generalised scaling relation (solid line) of the percolation parameters obtained from a conventional Seaton [8] analysis of the nitrogen sorption data obtained before (■) and after (◆) a mercury porosimetry experiment on a sample from batch Q2.

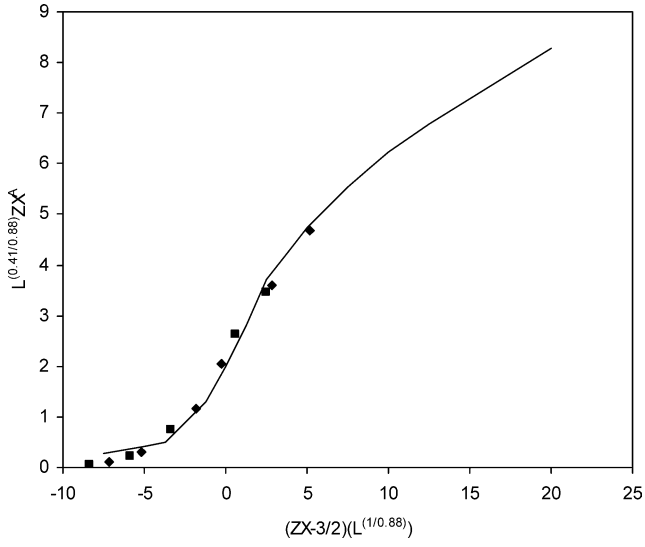

Fig. 8. Fits to the generalised scaling relation (solid line) of the percolation parameters obtained from a conventional Seaton [8] analysis of the nitrogen sorption data obtained before (■) and after (◆) a mercury porosimetry experiment on a sample from batch W1.

obtained before porosimetry. From Figs. 2 and 6 it can be seen that at smaller pore diameters the pore-diameter distributions obtained before and after porosimetry are identical, within experimental error. Deviations between the distributions obtained before and after porosimetry only occur for the largest diameter pores present in the samples. Figs. 2 and 6 indicate that batches Q2 and W1 meet the criteria described above for the application of the new analysis to determine pore-length distributions. For both Q2 and W1 the total intrapellet mercury intrusion volume is less than the corresponding cumulative mesopore volume from the BJH pore-diameter distribution. This finding, and the position of the sharp rise in each of the mercury intrusion curves, suggests that both Q2 and W1 are solely mesoporous. Hence the overall lattice size in these materials is likely to be the size of the whole pellet.

The sets of nitrogen sorption isotherms obtained before and after porosimetry were analysed using the conventional percolation analysis described by Seaton [8], and using the new method described above. The fits of the experimental data to the generalised scaling relation [Eq. (6)] are shown in Figs. 7–10. The values of the pore connectivity and lattice size obtained from the two approaches are shown in Tables 1

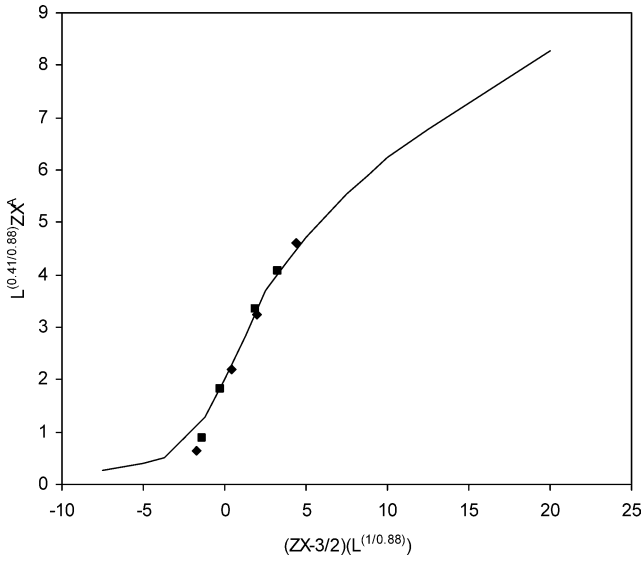

Fig. 9. Fits to the generalised scaling relation (solid line) of the percolation parameters obtained from the new analysis of the nitrogen sorption data obtained before (■) and after (◆) a mercury porosimetry experiment on a sample from batch Q2.

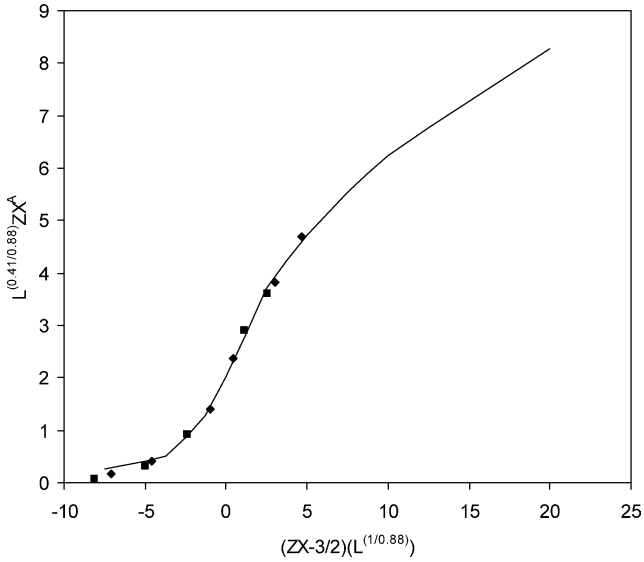

Fig. 10. Fits to the generalised scaling relation (solid line) of the percolation parameters obtained from the new analysis of the nitrogen sorption data obtained before (■) and after (◆) a mercury porosimetry experiment on a sample from batch W1.

and 2, for batches Q1 and W1, respectively. From Tables 1 and 2, it can be seen that the two approaches lead to very different estimates of the percolation parameters. Table 3 compares the values of the ratios Z_A/Z_B and T_A/T_B obtained from the conventional Seaton [8] analysis, and from the new method described above. It can be seen that, for each batch of pellets studied here, the conventional Seaton [8] analysis leads to values of the ratios Z_A/Z_B and T_A/T_B that are inconsistent with each other. The new analysis method inherently leads to consistent values of the ratios Z_A/Z_B and T_A/T_B. The values of T_A/T_B and Z_B obtained from the new

Table 1
Pore-connectivity and lattice size parameters obtained from the nitrogen sorption data for pellets from batch Q2

	Seaton [8] analysis		New analysis	
	Z (±0.1)	L (±0.1)	Z (±0.01)	L (±0.01)
Before porosimetry	4.1	7.0	3.00	5.00
After porosimetry	3.2	5.0	2.66	5.00

Table 2
Pore-connectivity and lattice size parameters obtained from the nitrogen sorption data for pellets from batch W1

	Seaton [8] analysis		New analysis	
	Z (±0.1)	L (±0.1)	Z (±0.01)	L (±0.01)
Before porosimetry	5.7	6.0	3.25	7.00
After porosimetry	4.3	5.7	2.82	7.00

Table 3
A comparison of the internal consistency of the conventional Seaton [8] analysis with that of the new analysis presented here. Also shown are the parameters of the pore-length distribution [Eq. (4)] obtained from the new analysis

Sample	Seaton [8] analysis		New analysis			
	Z_A/Z_B	T_A/T_B	Z_A/Z_B	T_A/T_B	$k/m^{1-\alpha}$	α
Q2	0.780	0.892	0.887	0.887	1.130×10^{-9}	−0.7
W1	0.754	0.844	0.868	0.868	4.280×10^{-13}	−1.1

analysis for each batch of pellets satisfy the condition given by Eq. (10). The typical linear dimensions of pellets from batches Q2 and W1 have been measured using callipers and found to be 4.1 ± 0.2 and 4.9 ± 0.2 mm, respectively. Also given in Table 3 are the parameters of the distribution of average pore length with diameter [Eq. (4)] obtained from the new analysis. It can be seen that, for both types of pellets, pore length is approximately inversely proportional to pore diameter. The pore length obtained by the new analysis is the typical distance between pore corrugations, or between junctions with pores of differing diameter. Typical pore lengths, obtained using the parameters in Table 3 in Eq. (4), for the samples studied here are of the order of several micrometres. This length seems to the authors to be unrealistically large for a single mesopore in an amorphous material. It is thus likely that the pore lengths obtained above for the materials studied here can only be treated as the pore lengths that are appropriate to an abstract network formed by using the new analysis to map the real pore structure onto a random pore-bond network model. Previous work [27,31] has shown that samples that give rise to anomalously low lattice sizes from the Seaton [8] percolation analysis possess macroscopic (∼ 0.01–1 mm) heterogeneities in the spatial distribution of pore diameter (or pore-surface area to volume ratio). In these types of materials pores of a similar size are grouped together within particular domains within the network. In nitrogen desorption these domains behave like a single pore in a pore-bond network. The values of the lattice size, obtained using both the original Seaton [8]

analysis and the new approach described above, and given in Tables 1 and 2 for the particular samples studied here, are all very low. Hence, the apparently large pore lengths from the new analysis may arise because the samples studied here have macroscopic structural heterogeneities. The "pore lengths" obtained are thus likely to be more characteristic of the typical length-scale of the macroscopic structural heterogeneities, rather than the actual length of a single pore. Materials, such as those studied by Seaton [8] (but not available to the authors), which produce much larger lattice sizes from the percolation analysis are also likely to give rise to lengths truly characteristic of individual pores from the new analysis method. A test for the complete correspondence of the random pore-bond network to the true pore structure of a real material has been given in previous work [31]. In addition, a method, only suitable to samples amenable to ^{1}H MRI, for correcting the results of the percolation analysis (and the new approach described above) for the effects of macroscopic heterogeneities has also been described in earlier work [31].

5. Conclusions

The analysis of two sets of nitrogen sorption data, taken from integrated nitrogen sorption and mercury porosimetry experiments on two types of catalyst support pellets, using the percolation theory developed by Seaton [8] leads to internal inconsistencies in the results. It is suggested that these inconsistencies, arising from the old theory, ultimately derive from the previous assumption that the average pore length is independent of pore diameter. A new analysis method has been presented that does not make this assumption and maintains the internal consistency of percolation theory when its application is extended to the data from integrated nitrogen sorption and mercury porosimetry experiments. The new analysis method allows the determination of the parameters of the distribution of average pore length with pore diameter, and also more accurate estimates of pore connectivity and lattice size.

Acknowledgment

This work has been supported by the EPSRC Grant GR/R61680/01.

References

[1] S. Brunauer, P.H. Emmett, E. Teller, J. Am. Chem. Soc. 60 (1938) 309.
[2] E.P. Barrett, L.G. Joyner, P.H. Halenda, J. Am. Chem. Soc. 73 (1951) 373.
[3] J.C.P. Broekhoff, J.H. de Boer, J. Catal. 10 (1968) 153.
[4] N.A. Seaton, J.P.R.B. Walton, N. Quirke, Carbon 27 (1989) 853.
[5] G.C. Wall, R.J.C. Brown, J. Colloid Interface Sci. 82 (1981) 141.
[6] G. Mason, J. Colloid Interface Sci. 88 (1982) 36.
[7] A.V. Neimark, Stud. Surf. Sci. Catal. 62 (1991) 67.
[8] N.A. Seaton, Chem. Eng. Sci. 46 (1991) 1895.
[9] J.H. Page, J. Liu, B. Abeles, H.W. Deckman, D.A. Weitz, Phys. Rev. Lett. 71 (1993) 1216.
[10] J.H. Page, J. Liu, B. Abeles, E. Herbolzheimer, H.W. Deckman, D.A. Weitz, Phys. Rev. E 52 (1995) 2763.
[11] L.F. Gladden, Chem. Eng. Sci. 46 (1991) 2455.
[12] R. Mann, P.N. Sharratt, Chem. Eng. Sci. 43 (1988) 1875.
[13] M.P. Hollewand, L.F. Gladden, Chem. Eng. Sci. 47 (1992) 1761.
[14] C. Rieckmann, F.J. Keil, Chem. Eng. Sci. 54 (1999) 3485.
[15] M. Sahimi, T.T. Tsotsis, J. Catal. 96 (1985) 552.
[16] J. Wood, L.F. Gladden, F.J. Keil, Chem. Eng. Sci. 57 (2002) 3047.
[17] S.V. Sotirchos, S. Zarkanitis, Chem. Eng. Sci. 48 (1993) 1487.
[18] R. Mann, J.J. Almeida, M.N. Mugerwa, Chem. Eng. Sci. 41 (1986) 2663.
[19] H. Liu, L. Zhang, N.A. Seaton, Chem. Eng. Sci. 47 (1992) 4393.
[20] H. Liu, L. Zhang, N.A. Seaton, J. Colloid Interface Sci. 156 (1993) 285.
[21] K.L. Murray, N.A. Seaton, M.A. Day, Langmuir 14 (1998) 4953.
[22] K.L. Murray, N.A. Seaton, M.A. Day, Langmuir 15 (1999) 6728.
[23] K.L. Murray, N.A. Seaton, M.A. Day, Langmuir 15 (1999) 8155.
[24] S.J. Gregg, K.S.W. Sing, Adsorption, Surface Area and Porosity, Academic Press, London, 1982.
[25] D. Stauffer, Introduction to Percolation Theory, Taylor & Francis, London, 1985.
[26] S.P. Rigby, R.S. Fletcher, J. Phys. Chem. B 108 (2004) 4690.
[27] S.P. Rigby, R.S. Fletcher, S.N. Riley, Chem. Eng. Sci. 59 (2004) 41.
[28] G.P. Androutsopoulos, R. Mann, Chem. Eng. Sci. 34 (1979) 1203.
[29] R.L. Portsmouth, L.F. Gladden, Chem. Eng. Sci. 46 (1991) 3023.
[30] N.C. Wardlaw, M. McKellar, Powder Technol. 29 (1981) 127.
[31] S.P. Rigby, Stud. Surf. Sci. Catal. 128 (2000) 111.
[32] S. Kirkpatrick, in: R. Balian, R. Mayward, G. Toulouse (Eds.), III-Condensed Matter, North Holland, Amsterdam, 1979, p. 321.